ACS OMEGA

Open Access

http://pubs.acs.org/journal/acsodf

Article

Single-Pass Demonstration of Integrated Capture and Catalytic Conversion of CO_2 from Simulated Flue Gas to Methanol in a Water-Lean Carbon Capture Solvent

Dushyant Barpaga, Jaelynne A. King, Jotheeswari Kothandaraman, Johnny S. Lopez, Benjamin M. Moskowitz, Michael L. Hubbard, Richard F. Zheng, Deepika Malhotra, Phillip K. Koech, Andy J. Zwoster, Robert A. Dagle, and David J. Heldebrant*

Cite This: *ACS Omega* 2024, 9, 46247−46262

Read Online

ACCESS | Metrics & More | Article Recommendations

ABSTRACT: Here, we demonstrate an integrated semibatch simultaneous CO_2 capture and conversion to methanol process using a water-lean solvent, *N*-(2-ethoxyethyl)-3-morpholinopropan-1-amine (2-EEMPA), that serves as both the capture solvent and subsequent condensed-phase medium for the catalytic hydrogenation of CO_2. CO_2 is captured from simulated coal-derived flue gas at a target >90 mol % capture efficiency, with a continuous slipstream of CO_2-rich solvent delivered to a fixed bed catalytic reactor for catalytic hydrogenation. A single-pass conversion rate >60 C-mol % and selectivity >80 C-mol % are observed for methanol at relatively low temperatures (<200 °C) in the condensed phase of the carbon capture solvent. Hydrogenation products also include higher alcohols (e.g., ethanol and propanol) and hydrocarbons (e.g., methane and ethane), suggesting that multiple products could be made offering adaptability with varied CO_2-derived products. Catalyst activity and selectivity are directly impacted by the water content in the capture solvent. Anhydrous operation provides high catalyst activity and productivity, suggesting that water management will be a critical parameter in real-world operation. Ultimately, we conclude that the integrated capture and catalytic hydrogenation of CO_2 are chemically viable and potentially more energetically efficient and cost-effective than conventional separate capture and conversion approaches.

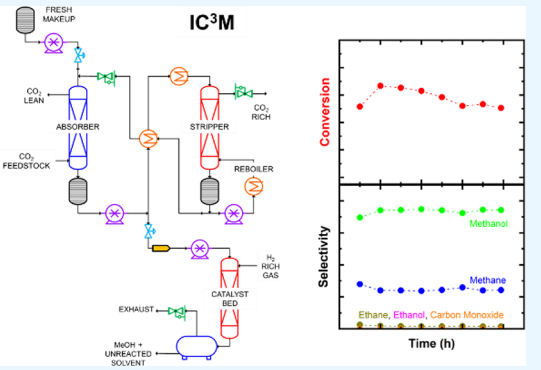

1. INTRODUCTION

Anthropogenic emissions of carbon dioxide (CO_2) into the atmosphere continue to drive global warming and climate change. Fossil fuels will be used until the world transitions to true carbon neutrality, necessitating the rapid deployment of carbon capture, utilization, and storage (CCUS). These technologies will be needed to minimize increases in global temperature to 1.5−2 °C above preindustrial times.[1−10] The most pressing need is emissions avoidance, which can be accomplished by capturing CO_2 from large point sources, i.e., postcombustion flue gases (containing 4−15% CO_2) from fossil-powered power plants, cement kilns, and steel manufacturing before it enters the atmosphere.[11−14] For industrial point sources, solvent-based postcombustion CO_2 capture technologies using amines (e.g., monoethanolamine [MEA]) are the most mature and are considered the industrial benchmark,[15−19] although there are promising advanced solvents, solid sorbents,[20,21] and membrane technologies[22] under development. Once point-source capture is achieved, technologies enabling negative emission, such as direct air capture of CO_2 (~400 ppm) coupled with permanent geological sequestration, are envisioned. In the United States, tax credits such as 45Q have been introduced as an economic incentive to offset carbon capture and storage costs,[23] but economically profitable CCUS has remained elusive thus far.

As such, there is a strong push to chemically convert CO_2 into fuels and chemicals that could be sold, providing an economic incentive for carbon dioxide removal. CO_2 could become a renewable, abundant, and inexpensive C_1 source to produce value-added chemicals and fuels, such as formic acid, methanol, methane, ethanol, polycarbonates.[24−38] While these reduced forms of reconstituted CO_2 are not CO_2-negative, they remain attractive targets that can be sold globally at

Received: August 1, 2024
Revised: October 23, 2024
Accepted: October 25, 2024
Published: November 4, 2024

Scheme 1. Proposed Gas-Phase and Condensed-Phase Methanol Synthesis from CO_2 and H_2 (Republished from Reference 66 with Permission)

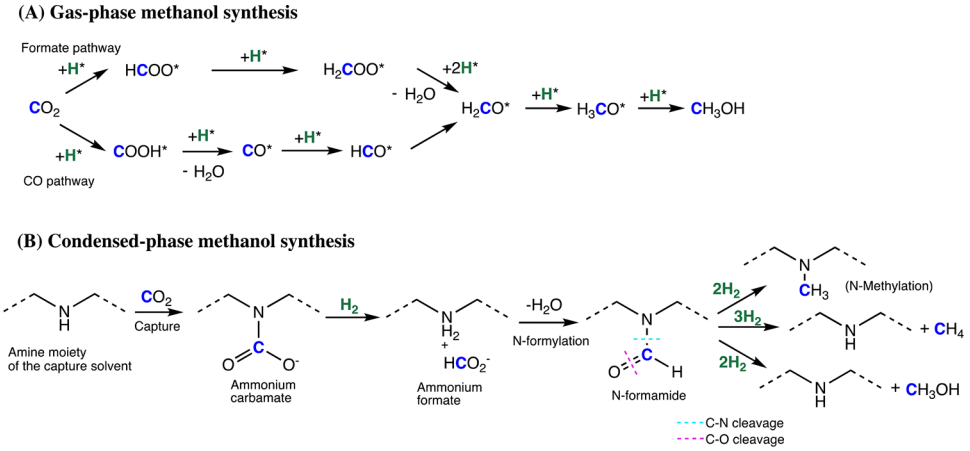

commodity scale enabling the establishment of the first CO_2 markets and economic incentives to pay for carbon capture and geological sequestration of the bulk of CO_2 captured.[39] While promising chemical transformations of CO_2 are on the horizon, the energetic and capital costs associated with using separate processes for capture, compression, transportation, storage, and then conversion of CO_2 are high. Natural processes, such as photosynthesis, couple the capture and conversion of CO_2 to biomass, minimizing inefficiencies in the two separate processes.

The field of CCUS has begun to focus on integrated capture and conversion of CO_2 to materials (IC^3M) as a way to produce CO_2-derived chemicals in a more efficient and economically feasible manner.[39−64] In the capture process, the primary energetic driver is the energy-intensive endothermic regeneration of the capture medium. In an IC^3M approach, coupling an exothermic chemical conversion of CO_2 with the regeneration of the capture medium could partially or, in some cases, fully offset these energy demands. In other words, if a fraction of captured CO_2 in the "condensed phase" is directly converted in the capture medium, then the energy associated with compression transportation, and storage of the remaining CO_2, is lessened. This provides significant energy and cost savings over conventional gas-phase conversions. Considering that the IC^3M process eliminates the energy needed for CO_2 desorption and CO_2 compression energies, IC^3M can reduce the energy consumption per metric ton of methanol by approximately 50% compared to the separate capture and conversion approach.[65] Moreover, the captured CO_2 (anionic carboxylates) is "activated" relative to molecular CO_2, thereby providing new reaction pathways and free-energy landscapes, creating enhanced reactivity and conversion at lower temperatures and pressures, and suppressing the undesirable, endothermic reverse water−gas shift reaction that limits conventional gas-phase processes.[39]

There has been a notable increase in the number of reports of CO_2 capture and conversion. However, most are not what we would define as an IC^3M approach as many of the amines and cosolvents are too volatile, costly, or viscous or lack the physicochemical properties needed for postcombustion CO_2 capture.[39−64] Only a handful of studies have demonstrated systems that we consider truly integrated. In these systems, the medium has been confirmed to efficiently perform the initial separation and capture from a point source or air, while also enabling electrocatalytic or thermocatalytic conversion of captured CO_2 directly into a value-added product. We have proposed that IC^3M could become a refinery of the future that produces multiple CO_2-derived material and financial incentives with market adaptability.[39]

As a step toward this goal, we have shown the viability of two integrated thermocatalytic process where CO_2 chemically bound in a leading water-lean postcombustion solvent, *N*-(2-ethoxyethyl)-3-morpholinopropan-1-amine (2-EEMPA), can be catalytically converted to CO_2-neutral fuels and chemicals.[39,62,66] First, 2-EEMPA was found to be a promising medium for producing synthetic natural gas at temperatures comparable to its own regeneration temperature.[62] The commercial Ru Al_2O_3 catalyst used in that work produced >90% conversion during the hydrogenation reaction. A technoeconomic analysis showed 12% lower synthetic natural gas selling price, a 5% increase in thermal efficiency, and a 32% reduction in capital expenditures (CAPEX) for an integrated capture and conversion system compared to a stepwise process.[62] By changing the catalyst from Ru/Al_2O_3 to Pt/TiO_2, we also demonstrated that CO_2 chemically bound in 2-EEMPA could be catalytically converted via C−N cleavage of the critical N-formamide intermediate at the same conditions, making methanol in both batch-wise and flow reactors.[66]

We also demonstrated how CO_2 captured in 2-EEMPA solvent could be converted to methanol when using the same IC^3M platform by changing the choice of catalyst and processing conditions (e.g., temperature, pressure, and H_2 feed concentration). The key enabling technology was identification of a suitable heterogeneous catalyst that facilitates both methanol formation while simultaneously allowing reuse of the solvent (after separately and recycle). To accomplish this, a TiO_2-supported Pt heterogeneous catalyst was developed that contains the suitable metal and acid−base properties to suppress *N*-methylation of the amine solvent, while also facilitating selective C−N cleavage to produce methanol. Scheme 1 illustrates the gas-phase and condensed-phase mechanisms, the latter using CO_2-captured amines, reported to facilitate the hydrogenation of CO_2 to methanol. Furthermore, we reported technoeconomic analyses that suggest methanol can be produced with a minimum selling price of $4.4/gallon ($1460/metric ton) when using CO_2 captured from a 650 MW natural gas combined cycle plant. We also reported how assumed but realistic improvements made to

https://doi.org/10.1021/acsomega.4c06919
ACS Omega 2024, 9, 46247−46262

space velocity and methanol selectivity could enable cost parity to fossil-derived methanol, with a selling price of ≈$1.4/gal ($470/metric ton).[66] However, while EEMPA has been shown to be a cost-effective and energy-efficient solvent for carbon capture and a promising solvent for catalytic reductions, our previous work had not yet experimentally demonstrated both capture and conversion steps together under sequential process operation. The envisioned integrated process had been reflected as a process model in prior work, which notably did include water management at scale to separate conversion products.[66]

In this work, we present the results and viability of an IC^{3}M process performing an integrated semibatch single-pass demonstration of both capture and conversion operating concurrently at realistic process conditions. CO_2 is first captured from a simulated coal-derived flue gas in a 5 L lab-scale continuous flow solvent-based absorption unit. From this absorber, a slipstream of CO_2-rich EEMPA is flowed through a packed bed catalytic reactor, co-fed with H_2, to produce methanol continuously in the condensed phase. We present results for catalyst activity, lifetime, productivity, product selectivity, and solvent durability under conditions relevant to real-world operation. We conclude with a discussion of process viability and the potential economic and energetic benefits of IC^{3}M as a carbon capture and valorization process.

2. EXPERIMENTAL METHODS

In our process, integrated CO_2 capture and conversion occur sequentially. First, the lean solvent absorbs CO_2, capturing it into the liquid phase. Then, a slipstream of the CO_2-rich solvent is routed through a continuous catalytic converter to generate value-added products. Two independent systems were plumbed together to develop this semiclosed loop integrated process (see Figure 1). The first is our laboratory-scale continuous flow system (LCFS) apparatus, which enables the continuous capture and separation of CO_2 from simulated flue gas. This unit was uniquely designed to mimic a traditional capture plant flowsheet to evaluate the continuous capture performance of novel solvent chemistries using reasonable solution volumes (∼3 L). For continuous operation, a separation process is required to regenerate the carrier capture solvent after passing through the catalytic conversion unit. This solvent contains a reduced concentration of CO_2 in liquid, which can then be recycled back into the absorber column. In our coupled system, a portion of the CO_2-captured solvent is then sent to the second unit, the thermocatalytic CO_2 conversion system (TCCS). There, CO_2-captured 2-EEMPA is sent to a packed bed reactor containing a heterogeneous multifunctional catalyst for conversion to methanol. A slipstream with a manually operated valve downstream of the CO_2-rich solvent pump is used to connect the LCFS unit to the TCCS unit. For TCCS, 2-EEMPA plays the role of a CO_2 carrier.

2.1. Capture Solvent Synthesis. The synthesis of 2-EEMPA solvent was performed as previously reported.[67] Briefly, 2-EEMPA was synthesized in a single step by the reaction of commercially available 3-aminopropylmorpholine and 2-bromoethyl ethyl ether, providing the product in good yields (86%).

2.2. LCFS. Details regarding the process equipment in the LCFS and a range of run conditions have been described in prior publications.[67−69] Briefly, the LCFS consists of an absorption and desorption/stripper column (both 3 in. in diameter and ∼20 in. high) through which a constant inventory of capture solvent, 2-EEMPA, recirculates. The absorber column is packed with two 8 in. pieces of Sulzer Mellapak 500.Y structured packing sections. The stripper column is packed with 0.24″ Pro-Pak 316 stainless steel Canon Instruments random packing material. The capture process in the LCFS is initiated in the absorber column with the interaction between the amine solvent and the CO_2-rich feedstock gas as the solvent flows down the column. The CO_2-rich solvent flows to the bottom of the absorber column and the gas feedstock, now with reduced CO_2 concentration, leaves out of the top of the absorber column. The CO_2-rich solvent is pumped from the absorber column to the top of the stripper column through a cross-flow heat exchanger. The average temperature of the stripper column is 105 °C with the heat sourced from the reboiler, which results in the thermal desorption of CO_2 from the CO_2-rich solvent. The stripper column maintains pressure from continuous release of CO_2 into the gas phase, providing a driving force for recirculation back into the absorber column via the cross-heat exchanger in the absence of a pump. The liberated CO_2 exits the column as a concentrated CO_2-rich gas.2.3.

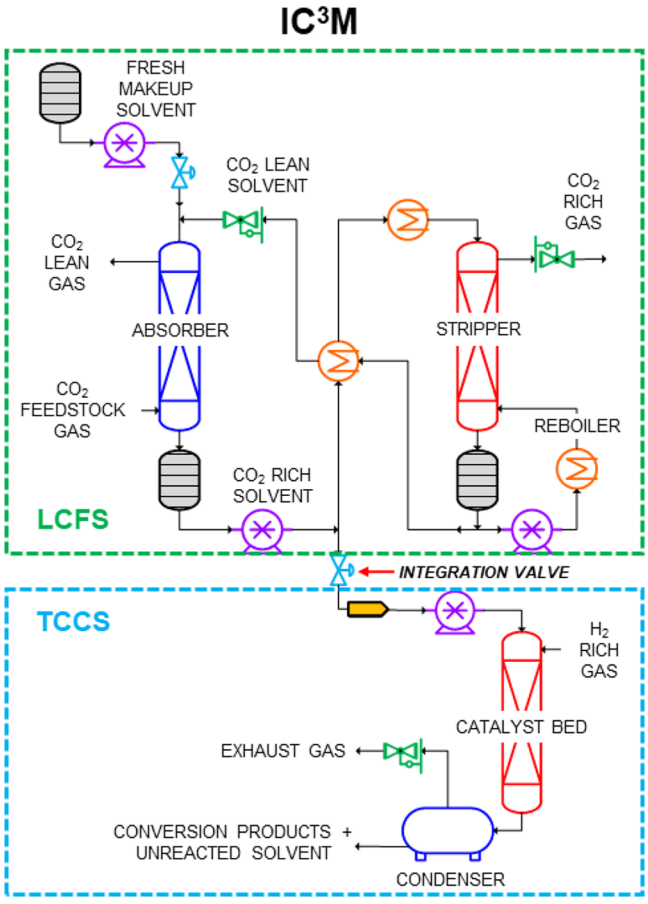

Figure 1. Process flow diagrams of the two independent bench-scale test systems, the laboratory-scale continuous flow system (LCFS) and the thermocatalytic CO_2 conversion system (TCCS), which together make up the IC^{3}M apparatus for combined capture and conversion of CO_2 to methanol.

2.3. TCCS. The TCCS consists of a temperature-controlled, pressurized, cylindrical packed bed (<10 g catalyst) within which the three-phase reaction takes place to selectively convert dissolved CO_2 into desired products. Details regarding

https://doi.org/10.1021/acsomega.4c06919
ACS Omega 2024, 9, 46247−46262

Table 1. Process Conditions at Steady State for LCFS during Demos 1, 2, and 3

LCFS process parameter		demo 1	demo 2		demo 3		units
			before regen	after regen	before regen	after regen	
feed	CO_2/N_2 [dry basis]	15/85	15/85	15/85	15/85	15/85	[mol %]
	dew point	15.6	15.6	15.6			[°C]
absorber	avg. temperature	32.3	31.8	31.7	32.4	32.7	[°C]
	avg. pressure	0.08	0.23	0.22	0.26	0.27	[psig]
stripper	avg. temperature	95.1	103.4	102.8	103.4	103.5	[°C]
	avg. pressure	14.4	14.8	14.9	15.1	15.3	[psig]
reboiler	temperature	114.9	116.6	115.6	116.1	116.2	[°C]
flow	liquid	15.3	12.6	12.8	11.9	11.5	[kg/h]
	gas	0.61	0.60	0.60	0.60	0.60	[kg/h]
	L/G	25.2	20.9	21.1	19.7	19.1	[-]

Table 2. Relevant Process Conditions in the TCCS for Demos 1, 2, and 3

TCCS process parameter		demo 1	demo 2		demo 3		units
			before regen	after regen	before regen	after regen	
temperature		170 °C	190 °C	190 °C	190 °C	190 °C	[°C]
water content in liquid feed		2	2	2	<0.1	<0.1	[wt %]
gas feed	H_2/N_2	93/7	93/7	93/7	93/7	93/7	[mol %]
	flow rate	5.9 E − 4	5.9 E − 4	5.9 E −4	5.9 E − 4	5.9 E − 4	[kg/h]
liquid feed	2-EEMPA/CO_2/H_2O	78/5/17	79/4/17	76/3/21	96/3/1	95/4/1	[mol %]
	flow rate	6.7 E − 3	6.7 E −3	6.7 E − 3	6.7 E − 3	6.7 E − 3	[kg/h]
reactor	temp.	170	190	190	190	190	[°C]
	pressure	865	865	865	865	865	[psig]
	catalyst	1	1	1	1	1	[g]
	WHSV	0.084	0.058	0.059	0.054	0.055	[g CO_2 fed/g cat × h]

the process equipment in the TCCS and the flow conditions utilized are more thoroughly described in the literature.[62] Briefly, continuous-flow experiments were performed in a stainless steel tubular reactor (3/8 in. outer diameter, 0.305 in. inner diameter) where the reactor wall was conductively heated via a 3 in.-height tubular stainless steel block wrapped with fiberglass heating tape. Liquid was continuously fed from the absorber column to the TCCS reactor using a Teledyne high-performance liquid chromatography pump. Gases were fed to the reactor using Brooks mass flow controllers at a high pressure. The product stream was condensed in a 50 mL condenser pot maintained at 7 °C by using recirculatory thermostat baths. Gas products were analyzed in situ using GC, while liquid products were analyzed ex situ using GC-FID. The current configuration of the TCCS only allows a single-pass operation such that the reaction products must be phase separated. It also requires further distillation of the liquid phase to separate the unreacted carrier capture solvent.

2.4. Integration of LCFS and TCCS: Process Conditions. The LCFS was operated independently from the TCCS under the conditions listed in Table 1 until the system reached steady-state operation. Steady-state CO_2 capture was determined by monitoring the absorber gas outlet CO_2 concentration and confirming that the concentration had not changed >5% over the course of ∼1 h. After steady-state carbon capture was achieved, the LCFS and TCCS were integrated with the opening of a two-way valve, which allowed the CO_2-rich solvent to be pumped from the bottom of the absorber column to the TCCS inlet. It is important to note that the typical solvent flow rates used in both the LCFS and TCCS setups currently in our lab are incompatible for seamless integration. Since they are significantly different in their existing configuration (the typical recirculation rate in LCFS is ∼2000× larger than that of TCCS), the current approach to integration involves making use of the large difference in scale by running the TCCS in single-pass mode and maintaining cyclic operation of the LCFS by introducing a fresh makeup solvent stream at the same flow rate as what is diverted into the TCCS.

The integrated system contained a total solvent inventory of ∼3 L, with >97% of solvent volume participating in continuous capture in the LCFS. The remaining <3% was routed for catalytic conversion in the TCCS over the course of the 8 h of operation. The gas feedstock used for the LCFS was a humidified mixture of CO_2/N_2 (15.07/84.93 mol % on a dry gas basis). The concentration of CO_2 in this feedstock was set to mimic the National Energy Technology Laboratory B11A baseline, which represents a subcritical pulverized coal power plant.[13] The concentration of water used in the inlet feed to the IC^{3}M apparatus was lower than typical flue gas concentrations to account for a routinely used prescrubber that reduces acid gas concentrations. To match the water concentration after this hypothetical prescrubber, a previously optimized humidification level corresponding to a dew point of 15.6 °C was used in some runs. The 95/5 mol % H_2/N_2 gas feedstock for the TCCS comprised was used for the catalytic hydrogenation of CO_2. Dilute concentrations of nitrogen were employed to facilitate quantification of the total gas flow out of the reactor. Since regeneration of the CO_2-carrier solvent is not the primary objective of this demonstration, the product liquid generated after the catalytic reaction was accumulated and analyzed without recycling or purification. Three demo (demonstration) experiments were performed to experimentally evaluate IC^{3}M to methanol in EEMPA. Approximately 1 g of solid crushed powder catalyst composed of 5 wt % Pt supported on TiO_2 was used in the TCCS for each experiment.

https://doi.org/10.1021/acsomega.4c06919
ACS Omega 2024, 9, 46247−46262

The conversion for "Demo 1" and "Demo 2" was performed with fresh catalyst at 170 and 190 °C, respectively. "Demo 2" is a repeat experiment of "Demo 1" with an extra step to regenerate the catalyst. Here, the spent catalyst was heated to 475 °C and oxidized for 1 h under a 10 vol % O_2/N_2 gas stream. This was followed by cooling to 120 °C and rereducing the catalyst for 8 h under a 10 vol % H_2/N_2 gas stream. "Demo 3" was performed under comparable conditions to Demo 2, but in anhydrous EEMPA to study the influence of water content entering from the LCFS capture unit. Demo 3 also included a second interval of catalytic conversion after catalyst regeneration similar to Demo 2 to study the influence of a higher regeneration temperature (550 °C held for >5 h). All other test parameters, including total solvent inventory, catalyst composition, capture conditions, and reaction pressures, were held constant between Demo 1, Demo 2, and Demo 3.

The relevant process conditions pertaining to the LCFS for each run are listed in Table 1. As intended, the steady-state values are consistent with each other for each Demo, including before and after regeneration. For a typical demonstration of the IC^{3}M, the run begins with an initial decoupled operation of both the LCFS and TCCS for a short period. During this period, the TCCS is brought up to pressure and temperature and the LCFS reaches a steady state. When the TCCS has reached desired operating conditions, coupled, integrated operation begins. During this period, a fraction of the CO_2-rich solvent is siphoned from the bottom of the absorber continuously into the TCCS at the conditions presented in Table 2. The table also includes weight hourly space velocity (WHSV) values based on the mass of CO_2 fed to the TCCS reactor. As soon as the CO_2-containing solvent reaches the catalyst bed, the hydrogenation reaction that converts CO_2 to various products occurs at the three-phase solid−liquid−gas interface. After hydrogenation, the product stream passes through a condenser trap to separate the condensed products, which are collected and sampled, from the gaseous products, which are sampled periodically and vented. Gas chromatography (GC) analysis of the exhaust gas from the TCCS reactor was sampled every 0.5 h to quantify the concentration of species such as unreacted H_2, thermally desorbed CO_2, inert N_2, and any gaseous products (CH_4, C_2H_6, CO, etc.). Raman spectroscopy chemometrics analysis[70] of the condensed liquid phase can identify presumably inert 2-EEMPA and unreacted dissolved CO_2, Karl Fisher analysis tracks H_2O concentration as a product of hydrogenation, and GC-FID analysis monitors condensable hydrogenation products of methanol and ethanol.

Additionally, liquid 1 mL aliquots were taken from the lean and rich solvent streams from the LCFS, as well as all of the condensed product solution from the collection pot downstream of the TCCS reactor. The LCFS liquid samples were characterized using Karl Fischer titration for water content as well as Raman spectroscopy for CO_2 and water content.[70] The hourly collected liquid products from the TCCS were measured by weight for mass balance and subsequently analyzed via a predetermined recipe on GC with flame ionization detection (GC-FID) for methanol and ethanol concentrations. They were analyzed via Karl Fischer titration for water content and NMR for carrier solvent stability analysis. The gas vents on the absorber and stripper columns were continuously monitored for CO_2 composition via infrared gas analyzers to quantify CO_2 capture efficiency.

After IC^{3}M demonstration completion, the spent catalyst was characterized using temperature-programmed oxidation mass spectroscopy (TPO-MS), diffuse reflectance infrared Fourier transform spectroscopy (DRIFTS), and/or powder X-ray diffraction (PXRD) for comparison with fresh unused catalyst.

2.5. Analytical Details. *IR CO_2 Analyzer.* The gas phase exiting the absorber column is analyzed in situ using a slipstream plumbed directly into a Quantek (Model 906E) portable IR analyzer calibrated for CO_2 detection in the concentration range of 0−20 vol %.

Gas Chromatography Coupled with a Flame Ionization Detector (GC-FID). Liquid product samples from the TCCS reactor were analyzed using an Agilent 6890GC instrument equipped with a flame ionizing detector. The column was an Agilent HP-5MS 30 m × 0.25 mm × 1.0 μm film thickness with a carrier gas of helium at 2.0 mL/min. The oven temperature was initially held for 5 min at 60 °C, ramped at 25 °C/min to 325 °C, with a final hold of 1 min. The inlet was heated at 260 °C and 1 μL of the sample was injected.

Nuclear Magnetic Resonance (NMR). ^{1}H NMR spectra of the liquid product from the TCCS carts were recorded on a 500 MHz Bruker NMR spectrometer in deuterated acetonitrile.

Raman Spectroscopy. A MarqMetrix Raman spectrometer with a liquid flow cell was used to record Raman spectra of the liquid samples collected from the LCFS system and TCCS cart. Spectra were recorded by using a laser power of 450 mW with an integration time of 200 ms. The flow cell was rinsed with methanol before and after the samples. A precalibrated chemometrics analysis model for CO_2 and water content was applied to the Raman spectra.[70]

Karl Fischer (KF) Titration. A Mettler-Toledo Coulometric KF Titrator was used to quantify the water content in each sample collected from the CO_2-rich and CO_2-lean streams in the LCFS cart, as well as the product liquid samples from the TCCS reactor.

GC. Analysis of the gas phase products from the catalysis bed was performed in situ using an Inficon Micro GC. The injector pulled samples for 30 ms with a backflush time of 12 s with a heater at 90 °C. Two columns were used to characterize the gas product: column A and column B. Column A utilized an Rt-Molsieve 5A column at a pressure of 45 psig and a temperature of 60 °C with an argon carrier gas. Column B utilized a Rt-Q-Bond column at a pressure of 25 psig and a temperature of 60 °C with a helium carrier gas. Automated injections occurred every 0.5 h. The GC was calibrated using a mixed gas cylinder containing light hydrocarbons including relevant compositions of H_2, N_2, CH_4, CO, CO_2, and C_2H_6.

Temperature-Programmed Oxidation Mass Spectrometry (TPO-MS). TPO was performed in a fixed bed quartz reactor (inner diameter of 10 mm) with plug flow fluid dynamics. 50 mg of spent Pt/TiO_2 was loaded into the reactor. The reactor was located within a resistively heated furnace with its temperature controlled by a digital feedback controller (Omega, CN3251). Inside the quartz reactor, the sample was supported on a quartz frit, and the bed temperature was recorded using a K-type thermocouple placed at the center of the catalyst bed. The sample was treated in 50 cm^3 min^{-1} 10% O_2/He (OXARC, Certified Standard) and fed through a combined CO_2 and H_2O filter (Restek, 23843) at 20 °C for 40 min. Without any prior thermal pretreatment, the sample temperature was ramped to 600 °C at 10 °C min^{-1} and held at 600 °C for 20 min. Heated lines (80−110 °C) transferred effluent gases to an online mass spectrometer (MS) (Stanford

https://doi.org/10.1021/acsomega.4c06919
ACS Omega 2024, 9, 46247−46262

Research Systems, RGA 200). The m/z ratios and assigned molecules monitored were 4 (He), 18 (H_2O), 28 (CO), 30 (NO), 32 (O_2), 44 (CO_2), and 46 (NO_2). Quantitative analysis of the carbon laydown on the fresh and spent catalyst samples was determined from the TPO peaks corresponding to CO and CO_2 by using MSRESOLVE software.

Infrared Spectroscopy. A Nicolet iS50 spectrometer equipped with a Praying Mantis DRIFTS accessory was used to record absorbance spectra of the spent catalyst from demo 3. The spectra were recorded at room temperature in a dry nitrogen atmosphere. The sample was mixed with KBr to improve the spectral quality. The instrument resolution was 4 cm^{-1}, and 16 scans were coadded for the spectrum. IR spectra of the fresh and spent catalysts for demo 2 were recorded using a Bruker IFS 66/s spectrometer. The instrument resolution was 4 cm^{-1} with an 8 mm aperture, and 1042 scans were coadded for the spectrum.

PXRD. Fresh and spent Pt/TiO_2 catalysts used in demo 1 and demo 3 were characterized by PXRD to verify structural integrity and analyze phase composition. Prior to analysis, the spent catalysts were rinsed with ethanol to remove the EEMPA solvent and dried under vacuum. Experiments were performed with a Rigaku MiniFlex 600 X-ray diffractometer (Cu Kα, λ = 1.5406 Å). The sample was placed in a powder sample holder under ambient conditions, and a pattern was collected from the 2θ range of 20−80° with a step size of 2° min^{-1}.

Brunauer−Emmett−Teller (BET) Surface Area. Nitrogen adsorption was measured at 77 K with an automatic volumetric sorption apparatus (Micromeritics ASAP 2000). Samples were pretreated at 150 °C for 12 h under a vacuum. The surface areas were determined from adsorption values for five relative pressures (P/P_0) ranging from 0.05 to 0.2 using the BET surface method.

2.6. CO_2 Capture Efficiency. The primary metric of evaluation for the capture performance is defined as the CO_2 capture efficiency (CE), the difference in the CO_2 composition between the inlet and outlet vapor streams of the absorber. The expression used to evaluate CE is shown in eq 1, where $y_{CO2}^{ABS_{IN}}$ and $y_{CO2}^{ABS_{OUT}}$ represent the gas phase concentration of CO_2 (in mole fraction) entering and exiting the absorber column, respectively.

$$\mathrm{CE}(\%) = 1 - \left[\left(\frac{y_{CO2}^{ABS_{OUT}}}{y_{CO2}^{ABS_{IN}}}\right) \times \left(\frac{1 - y_{CO2}^{ABS_{IN}}}{1 - y_{CO2}^{ABS_{OUT}}}\right)\right] \times 100 \quad (1)$$

2.7. Catalyst Performance. The overall reaction performance can be summarized by three major metrics: conversion, selectivity, and catalyst productivity. The conversion of CO_2 is represented by the elemental carbon mole conversion as shown in eq 2, which can be defined as a ratio of converted stoichiometric product moles to the total carbon moles in CO_2 fed into the reactor. Note that the carbon moles from the carrier solvent, 2-EEMPA, are disregarded in this calculation, as it is assumed that the solvent composition does not change as a result of this hydrogenation reaction.

$$\text{conversion}[\text{mol}\%] = \frac{n_{C,CH_4}^{OUT} + n_{C,CO}^{OUT} + n_{C,C_2H_6}^{OUT} + n_{C,CH_3OH}^{OUT} + n_{C,C_2H_5OH}^{OUT}}{n_{C,CO_2}^{IN}} \times 100 \quad (2)$$

Subsequently, the selective conversion of a given species in this reaction, denoted simply as the selectivity of species X (as shown in eq 3), can be defined as the ratio of stoichiometric moles of carbon in the product for that species (as shown in eq 4) compared to the sum of all converted product carbon moles. Here, species X can be any one of the five major products observed from this reaction (X = CH_4, CO, C_2H_6, CH_3OH, C_2H_5OH) and A is the stoichiometric number of carbon moles in species X (ex. for CH_4, A = 1, for C_2H_6, A = 2, etc.). The catalyst productivity is defined by the total mass flow rate of CO_2 converted to the mass of catalyst utilized for a given duration of time (eq 5).

$$\text{selectivity of } X[\text{mol}\%] = \frac{n_{C,X}^{OUT}}{\frac{\text{conversion}}{100} \times n_{C,CO_2}^{IN}} \times 100 \quad (3)$$

$$n_{C,X}^{OUT} = A \times n_X^{OUT} \quad (4)$$

$$\text{catalyst productivity}\left[\frac{g\,CO_2\ \text{converted}}{g\ \text{catalyst} \times h}\right] = \frac{n_{C,CO_2}^{IN} \times \left(\frac{\text{conversion}}{100}\right) \times MW_{CO_2}}{m_{\text{catalyst}}} \quad (5)$$

The carbon, hydrogen, and oxygen balances were closed for demo 3 and found to be within 1, 6, and 1% error, respectively. This considers the CO_2 and H_2 feeds to the TCCS reactor and the resulting products. This represents our confidence in the reported CO_2 conversion, product selectivities, and catalyst productivity (within 6%).

3. RESULTS AND DISCUSSION

3.1. CO_2 CE. Based on LCFS operating conditions identified in Table 1, and online gas phase analysis of the absorber outlet, the steady-state CE for demo 1 was observed to be ∼88%. For demo 2 and demo 3, this value was closer to ∼92%. The increase is attributed to minor modifications to the set point conditions, specifically the solvent recirculation rate.

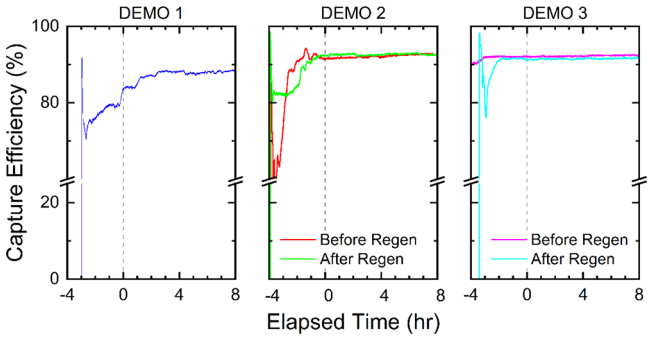

Figure 2. CO_2 capture efficiency data from the LCFS for demo 1, demo 2, and demo 3. [Demo 1: $T_{absorber}$ = 32.3 °C, $P_{absorber}$ = 0.08 psig, $T_{dewpoint}$ = 15.6 °C, $T_{stripper}$ = 95.1 °C, $P_{stripper}$ = 14.39 psig. Demo 2 before regeneration: $T_{absorber}$ = 31.8 °C, $P_{absorber}$ = 0.23 psig, $T_{stripper}$ = 103.4 °C, $P_{stripper}$ = 14.8 psig. Demo 2 after regeneration: $T_{absorber}$ = 31.7 °C, $P_{absorber}$ = 0.22 psig, $T_{dewpoint}$ = 15.6 °C, $T_{stripper}$ = 102.8 °C, $P_{stripper}$ = 14.9 psig. Demo 3 before regeneration: $T_{absorber}$ = 32.4 °C, $P_{absorber}$ = 0.26 psig, $T_{dewpoint}$ = N/A, $T_{stripper}$ = 103.4 °C, $P_{stripper}$ = 15.1 psig. Demo 3 after regeneration: $T_{absorber}$ = 32.7 °C, $P_{absorber}$ = 0.27 psig, $T_{dewpoint}$ = N/A, $T_{stripper}$ = 103.5 °C, $P_{stripper}$ = 15.3 psig]. The CO_2/N_2 in the gas feed for each demo was constant at 15/85.

https://doi.org/10.1021/acsomega.4c06919
ACS Omega 2024, 9, 46247−46262

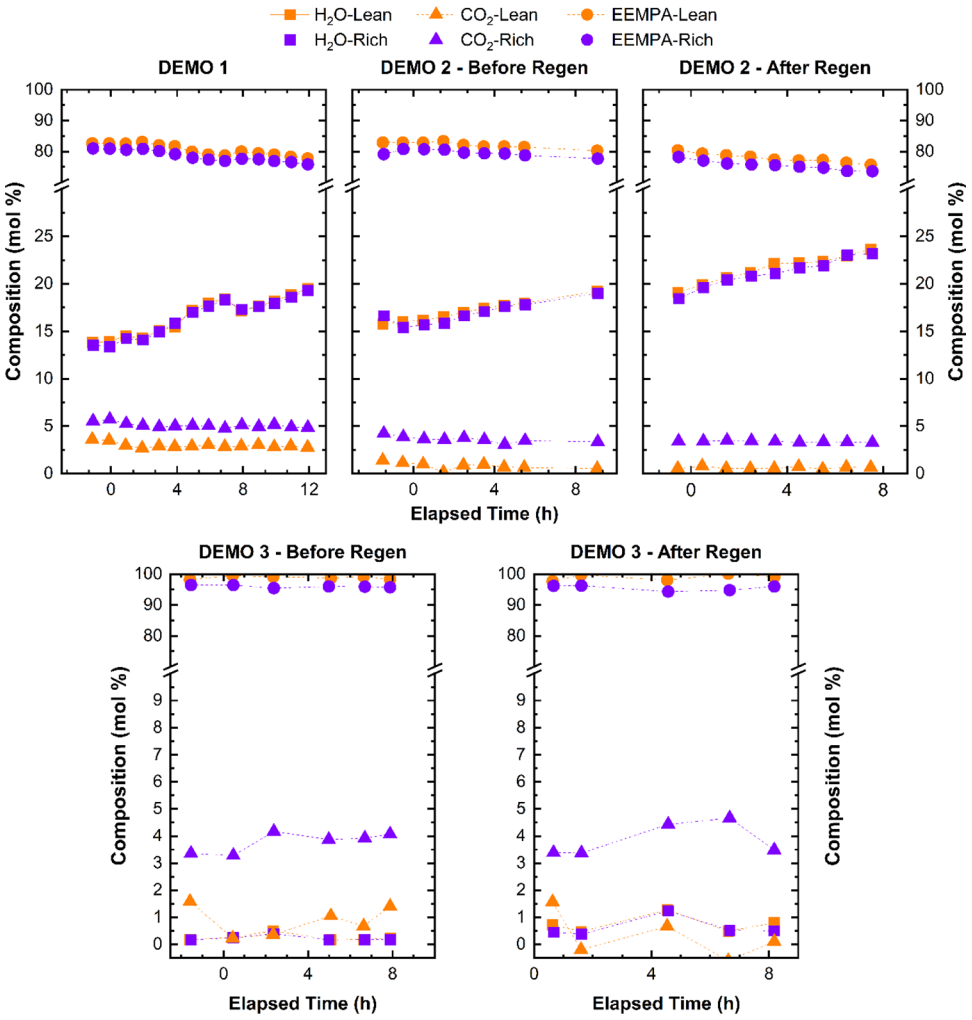

Figure 3. Liquid phase analysis from the LCFS for demos 1, 2, and 3. Experimental data is shown in points, with dashed lines added as a guide. [Demo 1: $T_{absorber}$ = 32.3 °C, $P_{absorber}$ = 0.08 psig, $T_{dewpoint}$ = 15.6 °C, $T_{stripper}$ = 95.1 °C, $P_{stripper}$ = 14.39 psig. Demo 2 before regeneration: $T_{absorber}$ = 31.8 °C, $P_{absorber}$ = 0.23 psig, $T_{stripper}$ = 103.4 °C, $P_{stripper}$ = 14.8 psig. Demo 2 after regeneration: $T_{absorber}$ = 31.7 °C, $P_{absorber}$ = 0.22 psig, $T_{dewpoint}$ = 15.6 °C, $T_{stripper}$ = 102.8 °C, $P_{stripper}$ = 14.9 psig. Demo 3 before regeneration: $T_{absorber}$ = 32.4 °C, $P_{absorber}$ = 0.26 psig, $T_{dewpoint}$ = N/A, $T_{stripper}$ = 103.4 °C, $P_{stripper}$ = 15.1 psig. Demo 3 after regeneration: $T_{absorber}$ = 32.7 °C, $P_{absorber}$ = 0.27 psig, $T_{dewpoint}$ = N/A, $T_{stripper}$ = 103.5 °C, $P_{stripper}$ = 15.3 psig].

It should be noted that at consistent process conditions, the CE is reproducible (before and after regeneration) and is very stable during the integration period.

As shown Figure 2, prior to integration (ET < 0 h), there is a transitory period during which the system is still approaching the steady state. During this period, recirculating solvent temperature in the LCFS is increasing to set point conditions and CO_2 loading is likely not stable. However, after integration with the TCCS (ET > 0 h), a steady state is achieved for the coupled capture and hydrogenation processes.

In addition to gas phase analysis that allows us to compute CE, liquid phase analysis of samples periodically collected from the lean and rich solvent streams in the LCFS allows us to track solvent composition to verify steady-state concentrations in the solution. Interpreting the rich solvent composition is critical for this integration, as it represents the composition of solvent entering the TCCS for conversion. For each run, the liquid phase in the LCFS has three components, 2-EEMPA, the solubilized H_2O, and the dissolved CO_2. We assumed that the concentration of any dissolved nitrogen in the solvent is negligible. Figure 3 summarizes the composition analysis of this three-component mixture for samples collected during each demo.

The data show that the H_2O content between the rich and lean solvents is similar at any given time. However, the H_2O concentration increases during operation, from 14 mol % during the start of demo 1 up to 24 mol % by the end of demo 2. The increase reflects the inability to maintain a water balance during steady-state operation via gas feedstock humidification. Since the analysis was not performed simultaneously with data collection, the imbalance could not be corrected during the run and was observed only after run completion. However, this increase in H_2O concentration does not impact capture performance as CE is stable during these runs. For demo 3, the water content remains minimal throughout the run. The CO_2 loading shown in Figure 3 is more stable in demo 3. As expected, the rich solvent has a higher CO_2 loading than the lean solvent, given the thermal desorption that occurs upstream of lean solvent sampling. For demo 1, the rich solvent CO_2 loading ranged from 5 to 5.5 mol %, while the rich solvent CO_2 loading ranged from 3.5 to 4 mol % for demos 2 and 3. These values for the rich solvent

https://doi.org/10.1021/acsomega.4c06919
ACS Omega 2024, 9, 46247−46262

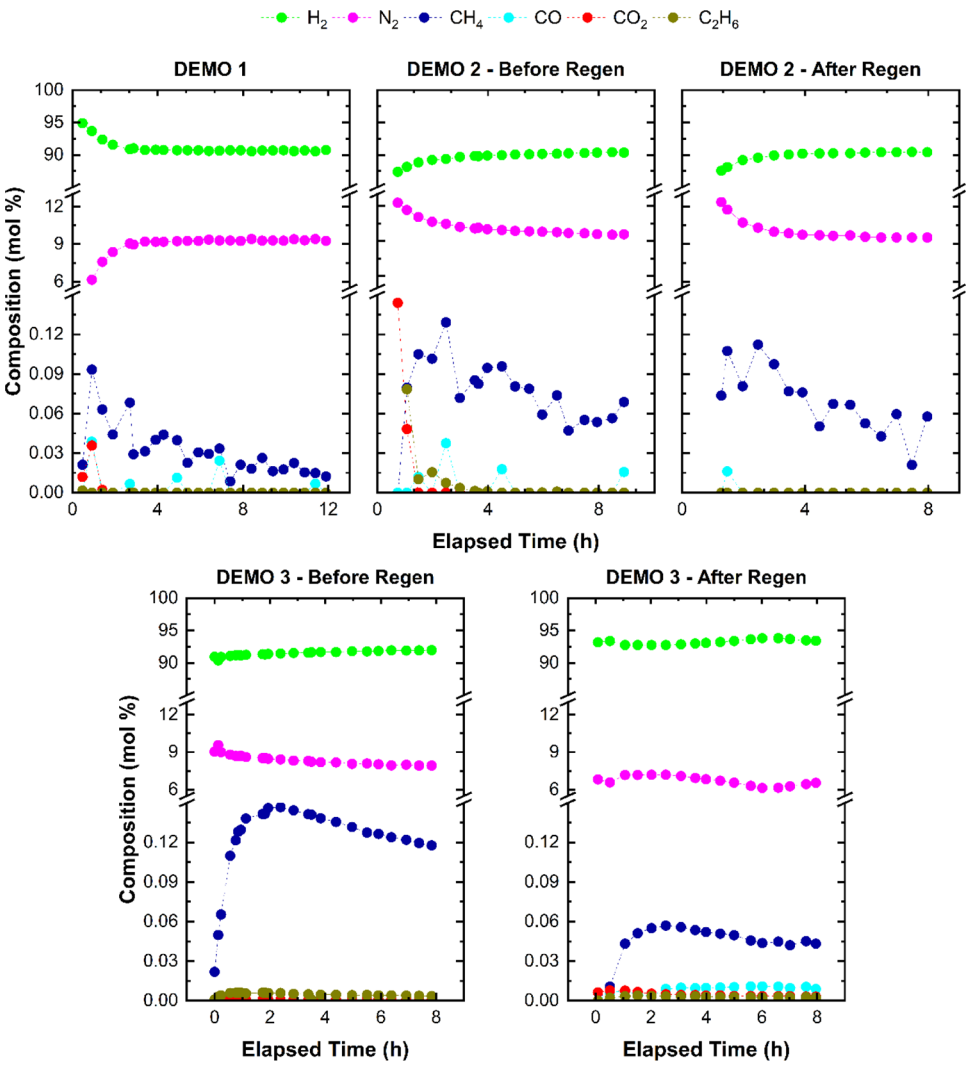

Figure 4. Gas phase analysis from the TCCS for demos 1, 2, and 3 showing the molar composition of sampled gas at periodic intervals during the runs. Experimental data are shown in points, with dashed lines added as a guide. [Demo 1: $T_{reactor}$ = 170 °C, $P_{reactor}$ = 865 psi, H_2O 17 mol %. Demo 2 before regeneration: $T_{reactor}$ = 190 °C, $P_{reactor}$ = 865 psi, H_2O 17 mol %. Demo 2 after regeneration: $T_{reactor}$ = 190 °C, $P_{reactor}$ = 865 psi, H_2O 21 mol %. Demo 3 before regeneration: $T_{reactor}$ = 190 °C, $P_{reactor}$ = 865 psi, H_2O 1 mol %. Demo 3 after regeneration: $T_{reactor}$ = 190 °C, $P_{reactor}$ = 865 psi, H_2O 1 mol %].

represent the concentration of CO_2 fed into the TCCS catalytic reactor.

3.2. Catalyst Performance. A slipstream of the CO_2-rich solvent from the LCFS was routed through the TCCS to demonstrate sequential capture and conversion steps sequentially. In the TCCS reactor, the CO_2-rich EEMPA solvent undergoes hydrogenation to produce methanol (EEMPA-CO_2^- + $3H_2$ → CH_3OH + H_2O + EEMPA). While methanol is our target product, the gas and liquid phase analyses also revealed the presence of other value-added products, including methane and ethanol. Figure 4 shows a summary of the gas phase analysis of the effluents from the TCCS reactor.

Compared to the feedstock concentration of H_2 at 93 mol %, the product gas stabilizes at a slightly lower H_2 concentration of ∼91 mol % for all runs indicating the consumption of H_2. The overall composition of all gaseous reaction products is <0.15 mol %, which is not unusual given the low concentration of dissolved CO_2 in the liquid feedstock. Of the three observed gas products, the CH_4 concentration is the highest but decreases as the reaction proceeds. It should be noted that in the absence of significant water loading on the carrier solvent (demo 3), methanation is more productive before catalyst regeneration. Additionally, low CO signals are periodically observed in demo 3, possibly from the endothermic reverse water−gas shift reaction, given the unique operating conditions including an active catalyst, high hydrogen gas phase partial pressure to CO_2 ratio, and efficient CO removal.[71,72]

The C_2H_6 product was more prominent in the initial stages of the higher temperature runs and is more prominent in the absence of water. Gas phase CO_2 is not present in significant quantities in the gaseous product stream for all demos, with only a small concentration observed in the initial hours of operation in demo 2. This may be due to the higher temperature of the reaction in demo 2 that may increase the thermal desorption of CO_2. Given the lack of significant CO_2 concentration observed in the product gas phase overall, it can be inferred that either (1) the dissolved CO_2 reacts in solution with the H_2 without first thermally desorbing, (2) any thermally desorbed CO_2 subsequently reacts in the gas phase or adsorbed phase of Pt/TiO_2 to form the observed products, (3) any unreacted CO_2 remains dissolved in the liquid phase, or, the most likely scenario, (4) a combination of all the above.

https://doi.org/10.1021/acsomega.4c06919
ACS Omega 2024, 9, 46247−46262

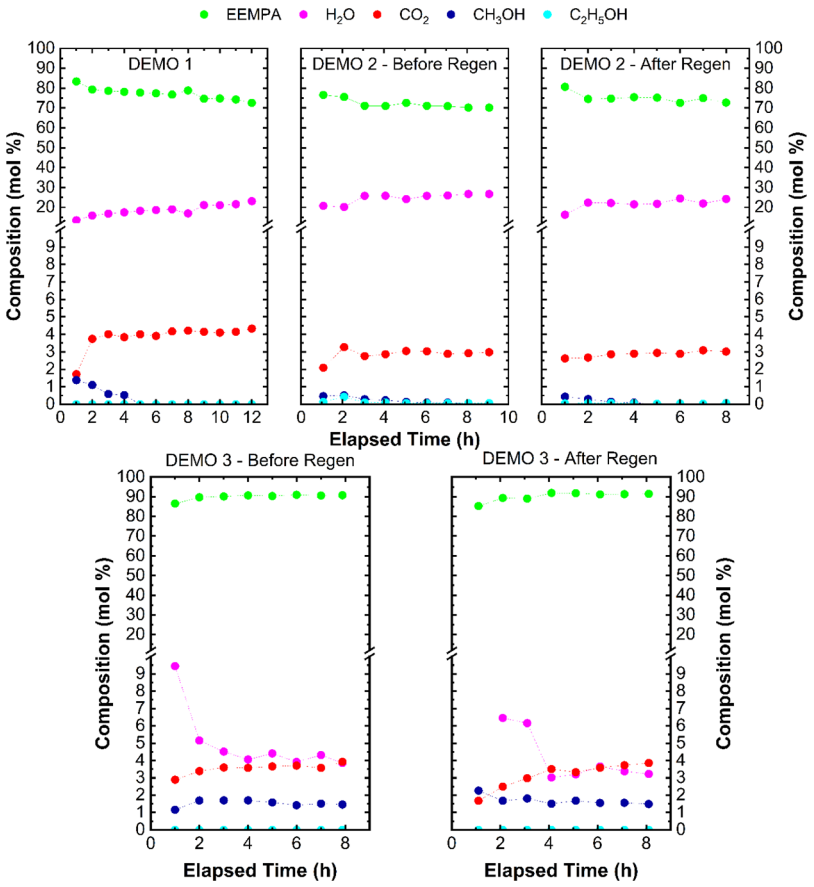

Figure 5. Liquid phase analysis from the TCCS for demos 1, 2, and 3 showing the molar composition of liquid sampled at periodic intervals during the runs. Experimental data is shown in points, with dashed lines added a guide. [Demo 1: $T_{reactor}$ = 170 °C, $P_{reactor}$ = 865 psi, H_2O 17 mol %. Demo 2 before regeneration: $T_{reactor}$ = 190 °C, $P_{reactor}$ = 865 psi, H_2O 17 mol %. Demo 2 after regeneration: $T_{reactor}$ = 190 °C, $P_{reactor}$ = 865 psi, H_2O 21 mol %. Demo 3 before regeneration: $T_{reactor}$ = 190 °C, $P_{reactor}$ = 865 psi, H_2O 1 mol %. Demo 3 after regeneration: $T_{reactor}$ = 190 °C, $P_{reactor}$ = 865 psi, H_2O 1 mol %].

Figure 5 shows a summary of the liquid phase analysis of the effluents from the TCCS reactor. In the presence of a higher water composition, the increase in reaction temperature from 170 °C in demo 1 to 190 °C in demo 2 has a minimal impact on the liquid products generated. However, the absence of water in the rich solvent stream in demo 3 significantly impacts the liquid products generated. Although the plotted data in Figure 5 shows the molar composition of the stream where the 2-EEMPA concentration varies due to the other components in the solvent, we assume that the net molar flow rate of 2-EEMPA is the same going into and exiting the reactor. This encompasses the underlying assumption that the reaction temperature does not degrade the carrier solvent and that it is thermally stable at relevant temperatures. This assumption is corroborated with ^{1}H NMR analysis of the liquid product collected from demo 3 (Figure 6), which matched the as-synthesized solvent, confirming the stability of 2-EEMPA during the catalysis reaction under these conditions.

Additionally, NMR analysis (Figure 6) also showed (1) no degradation products of 2-EEMPA and (2) the presence of methanol (peak at 3.3 ppm) in the liquid product, consistent with the GC-FID results presented here in Figure 5. We note that the peak at ∼2.3 ppm in the fresh solvent corresponds to the N−H proton of EEMPA. Because this proton is highly sensitive to its environment due to hydrogen bonding, it cannot be detected in the spent solvent because of fast proton exchange.

The water concentrations after catalysis for both demo 1 and demo 2 are shown to increase compared to the concentration in rich solvent entering the TCCS. This is attributed to the net production of H_2O as a byproduct of the hydrogenation reaction. This is especially noticeable in demo 3 analysis as there is minimal water (<1 mol %) entering the TCCS, but up to 10 mol % water in the effluent product. Interestingly water production is higher in the early stages of the run, indicating dynamic changes in the extent of byproduct reactions during operation. The dissolved CO_2 concentration in the liquid phase TCCS product stream decreases compared to the concentration in the rich solvent exiting the LCFS absorber column (Figure 3), corresponding to the expected consumption of CO_2 in the TCCS. In addition to water, methanol is one of the primary observed liquid products, especially at a lower reaction temperature (demo 1). A relatively small amount of ethanol production is observed only in the higher temperature run (demo 2).

Importantly, the lower water composition in the solvent for demo 3 clearly affects the production of methanol. In general, the water content in the solvent entering the catalysis reactor adversely affects the yield of methanol. For the runs (demos 1 and 2) that had water in the inlet solvent, the selectivity of methanol over the course of the experiment was relatively low and/or quickly reduced to minimal as the reaction progressed. For the run without water (demo 3), the selectivity of methanol was much higher (∼2 mol %) and consistently

https://doi.org/10.1021/acsomega.4c06919
ACS Omega 2024, 9, 46247−46262

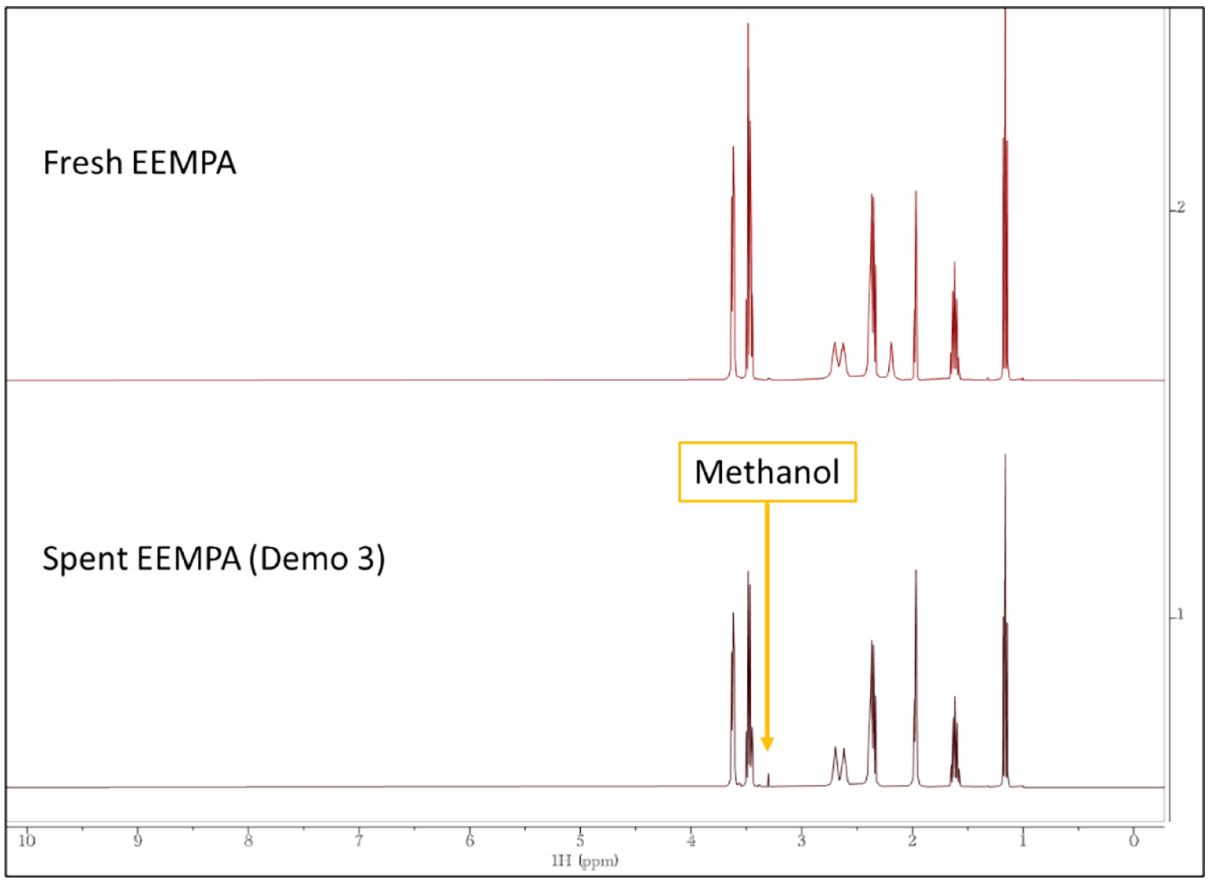

Figure 6. ^{1}H NMR analysis of liquid product from demo 3 as compared to fresh solvent.

maintained over the course of the experiment. It should be emphasized that these results confirm successful capture and conversion of CO_2 via this unique integrated methodology, corroborating our previous ex situ batch experiments. The additional, subsequent catalyst performance analysis evaluates the nonoptimized reaction conditions and parameters used in these initial runs to establish a path forward for future studies.

Combining the time-dependent gas and liquid analysis, the conversion and corresponding selectivity for product species can be represented as a function of elapsed reaction time for demos 1, 2, and 3 (Figure 7). The higher reaction temperature in demo 2 yielded higher overall conversion compared to demo 1 during the initial few hours of reaction before catalyst activity decreased. Catalyst activity was not maintained for the duration of the experiment for demos 1 and 2.

Instead, conversion rapidly decreases from as high as 35−50 mol % to <10 mol % within ∼4 h of reaction. This rapid reduction in conversion is more prominent for the lower reaction temperature (demo 1). Conversion after regeneration of catalyst in demo 2 is lower than fresh catalyst conversion, suggesting that the specific procedure used to regenerate the catalyst for this run was not sufficient to reproduce the same catalytic activity. The spent catalyst likely needed to be oxidized at high temperature for a longer time than the 1 h activation period used in demo 2. Moreover, the presence of significant water in the reactant feed may contribute to the poisoning of the catalyst and hinder conversion. This is confirmed by the results of demo 3, where longer/hotter regeneration conditions and, more importantly, the absence of water in the solvent feed for TCCS yield much higher conversion (∼60 mol %) that is maintained through the course of operation.

For the reaction at 170 °C (demo 1), the catalyst is initially more selective toward the production of methanol (with selectivity as high has ∼90%). Conversion significantly decreases to <10% after approximately 6 h of time on stream, due to catalyst deactivation whereby only a small amount of methane is produced. At 190 °C (demo 2), the selectivity of the catalyst is altered such that in addition to methanol, ethanol and more methane are also produced. Regeneration of the spent catalyst seems to further inhibit methanol production more rapidly, favoring increased methane and ethanol production. The decay in methanol selectivity over the course of operation for demo 1 and demo 2 is likely significantly impacted by the presence of water. In demo 3, high selectivity (>70 mol %) is maintained throughout. Moreover, catalyst regeneration appears to improve the methanol selectivity to ∼80 mol % while decreasing methane selectivity.

Figure 8 summarizes catalyst productivity for demos 1, 2, and 3, which has an observed trend similar to that of CO_2 conversion. This allows for comparison of runs based on catalyst amount. The productivity can also be used as a comparison with larger-scale reactions to evaluate industrial viability. At peak activity, the productivity of the catalyst is as high as ∼0.06 g of CO_2 converted/g of catalyst·h at initial operation. For demos 1 and 2, the productivity remains <0.02 g CO_2 converted/g catalyst·h throughout the course of operation. Between the two, a higher reaction temperature seemingly leads to lower productivity even though conversion is higher. This indicates an unsurprising trade-off for

https://doi.org/10.1021/acsomega.4c06919
ACS Omega 2024, 9, 46247−46262

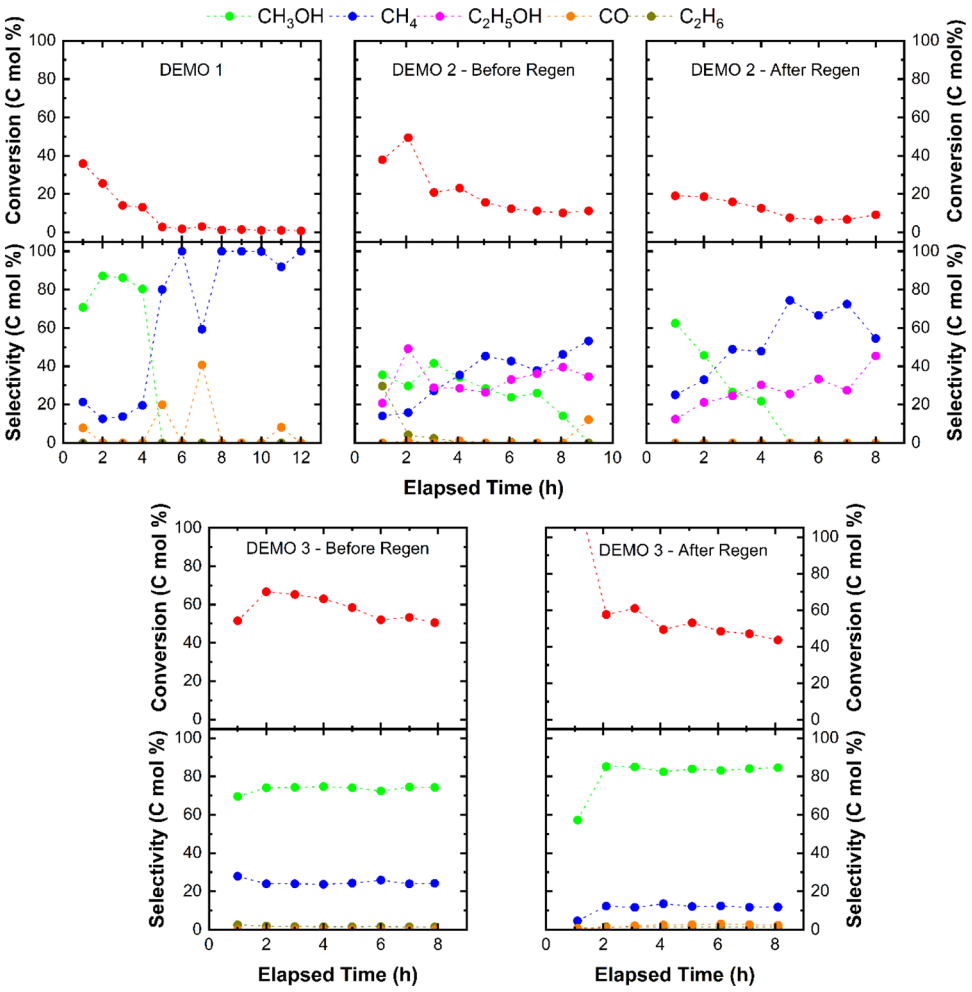

Figure 7. CO_2 conversion and product species selectivity as a function of reaction time on stream during demos 1, 2, and 3. Computed experimental data is shown in points, with dashed lines added as a guide. [Demo 1: $T_{reactor}$ = 170 °C, $P_{reactor}$ = 865 psi, H_2O 17 mol %. Demo 2 before regeneration: $T_{reactor}$ = 190 °C, $P_{reactor}$ = 865 psi, H_2O 17 mol %. Demo 2 after regeneration: $T_{reactor}$ = 190 °C, $P_{reactor}$ = 865 psi, H_2O 21 mol %. Demo 3 before regeneration: $T_{reactor}$ = 190 °C, $P_{reactor}$ = 865 psi, H_2O 1 mol %. Demo 3 after regeneration: $T_{reactor}$ = 190 °C, $P_{reactor}$ = 865 psi, H_2O 1 mol %].

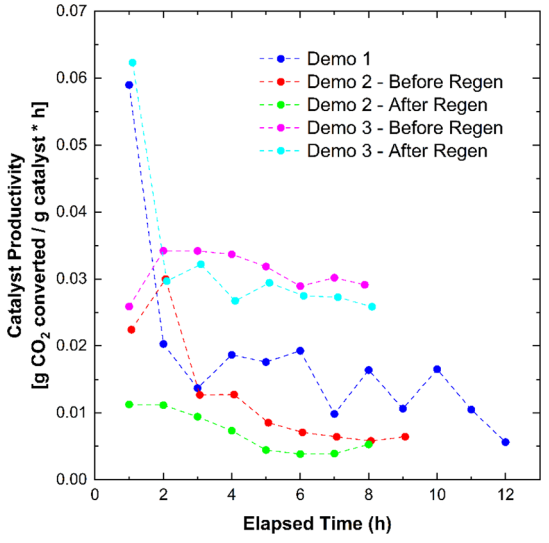

Figure 8. Catalyst productivity for demos 1, 2, and 3 as a function of elapsed reaction time. Experimental data are shown in points, while dashed lines are added just as a guide.

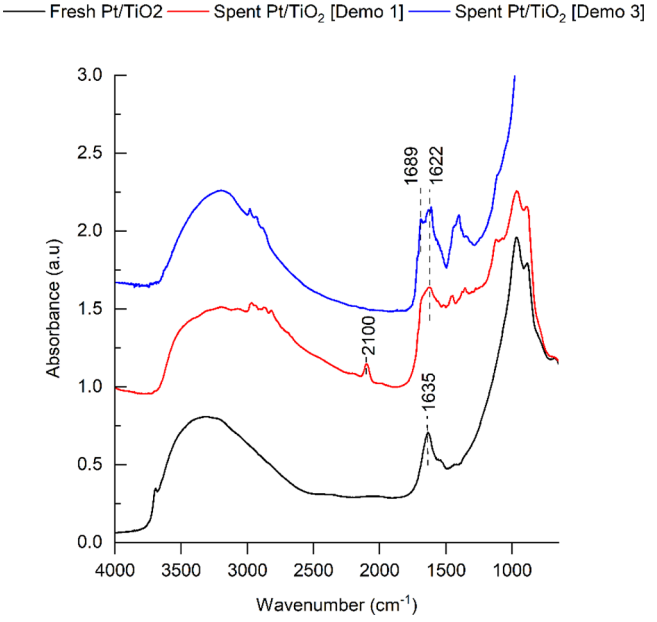

Figure 9. DRIFTS spectra of the fresh and spent Pt/TiO_2 catalysts.

https://doi.org/10.1021/acsomega.4c06919
ACS Omega 2024, 9, 46247−46262

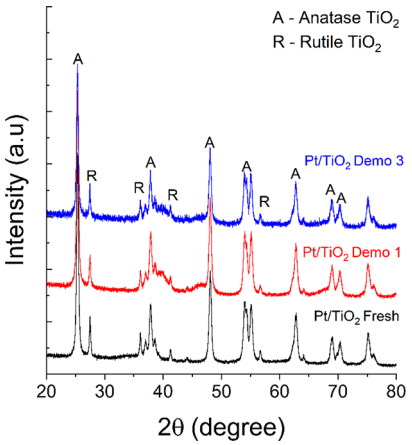

Figure 10. PXRD patterns of fresh and spent Pt/TiO_2 catalysts.

productivity vs conversion as a function of reaction temperature. Alternatively, when minimal water is present in the TCCS (demo 3), productivity steadies at ~0.03 g CO_2 converted/g catalyst·h. A lack of water clearly minimizes catalyst poisoning and benefits productivity.

3.3. Spent Catalyst Characterization. To understand the mechanism of deactivation of the catalyst, we characterized the spent and fresh catalysts by DRIFTS, PXRD, BET, and TPO-MS.

DRIFTS characterization shows the different adsorbed species between the demo 1 spent catalyst and the demo 3 spent catalyst (Figure 9). Spent catalysts showed C−H bands (~3000−2800 cm^{-1}) corresponding to the capture solvent EEMPA. The demo 1 catalyst showed a strong band corresponding to terminal Pt-CO at 2100 cm^{-1}. In the demo 1 and 3 spent catalysts, we observed bands between 1700 and 1200 cm^{-1} that are likely bicarbonate and carbonate. The bicarbonate and carbonate may be related to water in the feedstock, particularly in the case of demo 1. Water could react with the captured CO_2 to form bicarbonates and carbonates (carbamate/CO_2 + H_2O → HCO_3^-/CO_3^-) that bind strongly with the catalyst at low reaction temperatures. In demo 3, bicarbonate and carbonate are likely formed by the reaction of captured CO_2 with lattice oxygen sites and hydroxyls on the anatase TiO_2 surface (or less likely with byproduct formation of H_2O).[73]

Table 3. Carbon Content Analysis (wt %) for the Fresh, Spent after Demo 1, and Spent after Demo 3 Catalyst Samples[a]11

catalyst sample (5 wt % Pt/TiO_2)	carbon content (wt %)
fresh	0.2
spent demo 1	2.2
spent demo 3	0.8

[a]Determined from the quantitative analysis of the TPO-MS data shown in Figure 11.

The fresh and spent (demos 1 and 3) catalysts showed similar PXRD patterns (Figure 10). Peaks corresponding to Pt particles were not seen in the PXRD given their small crystallite size, which remains below the detection limit. A strong diffraction pattern corresponding to the anatase phase of the TiO_2 support was observed in both the fresh and spent catalysts, in addition to minor peaks for the rutile phase. The TiO_2 support phases remain constant in all of the cases. The BET surface area of the fresh 5 wt % Pt/TiO_2 catalyst is 57.1 m^2/g.

TPO-MS analysis of the fresh catalyst showed minimal concentrations of H_2O and CO_2 (see Figure 11). The spent catalyst showed significant liberation of H_2O, CO_2, and CO starting at 100 °C. This indicates that carbon-containing species were sorbed on the catalyst, which could be oxidized to CO and CO_2 in the presence of O_2. It is interesting to note that significantly more CO_2 liberation was observed on the spent catalyst after demo 1 compared to demo 3. Quantitative analysis of this TPO-MS analysis indicates that the amount of carbon laydown present on the spent demo 1 and demo 3 catalysts was 2.2 and 0.8 wt %, respectively (see Table 3). This corroborates our conversion performance data, which indicated that much more captured CO_2 in the solvent was converted in demo 3. The source of CO_2 observed in this analysis can be attributed to the decomposition of sorbed bicarbonate and carbonate species on the catalyst surface. Given the lack of NO observed from the TPO-MS analysis, it can be assumed that negligible solvent adsorption occurred on the catalyst surface. The peak for CO_2 liberation for the demo

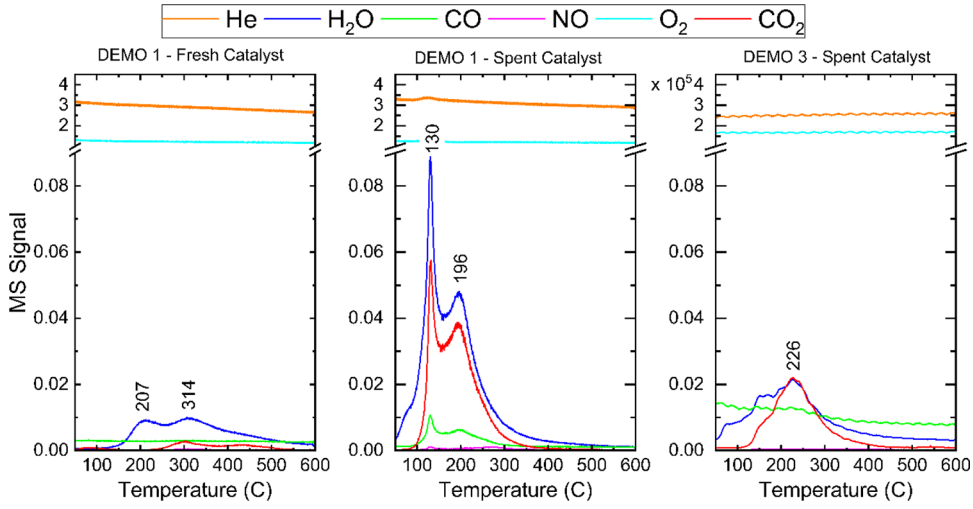

Figure 11. Temperature-programmed oxidation mass spectrometry (TPO-MS) analysis for the fresh (left), spent after demo 1 (middle), and spent after demo 3 (right) Pt/TiO_2 catalysts. TPO conditions for all experiments used 10% O_2/He stream at 50 cc/min ramping at 10 °C/min.

https://doi.org/10.1021/acsomega.4c06919
ACS Omega 2024, 9, 46247−46262

3 catalyst occurred at a much higher temperature (~226 °C) than the demo 1 catalyst (~130−196 °C), likely corresponding to the minimal residual sorbed bicarbonate and carbonate species that remain tightly bound to the demo 3 catalyst. Together, DRIFTS, TPO-MS, and conversion results suggest that the presence of water in the feedstock enriches the formation of carbonates and blocks the catalyst active sites. In addition, the DRIFTS and TPO-MS results indicate that the excess carbonate concentration on the catalyst surface likely converts to CO, which can strongly bind to Pt and deactivate the catalyst.

Overall, the observed catalytic deactivation during operation in the presence of water presents two approaches for next steps: (1) identify a new catalyst that is optimized for higher selectivities even in the presence of water or (2) reduce the water concentration in the feedstock for the IC^{3}M process. Future studies will address both approaches to not only optimize alternate catalyst formulations but also identify whether reducing the water concentration in the feed can be justified by projected process economics. Future experimental work on the IC^{3}M apparatus will also involve a revised flowsheet where the TCCS does not need to operate in single-pass mode, enabling the capture solvent to be recycled into the LCFS for closed loop operation.

4. CONCLUSIONS

In summary, we have demonstrated the viability of a simultaneous, integrated semibatch postcombustion capture, and catalytic reduction of CO_2 to methanol in the condensed phase of a single-component water-lean diamine solvent, 2-EEMPA. 2-EEMPA achieved steady-state carbon capture from simulated coal flue gas (CO_2, N_2 H_2O) with >90 mol % capture efficiency. A slipstream of a CO_2-rich solvent was pumped through a single-pass fixed bed catalytic reactor packed with Pt/TiO_2 fed with H_2 gas. Single-pass conversion rates of CO_2 reached >60 C-mol % with methanol selectivities greater than 80 C-mol % at relatively low temperatures (190 °C) in the condensed phase with negligible solvent decomposition. Other hydrogenation products detected include ethanol, methane, ethane, and carbon monoxide, with distributions that are sensitive to changes in hydrogenation temperature and water content. This sensitivity suggests that process conditions could be optimized to alter product distribution, providing some degree of market adaptability to adjust to changes in reagent or product pricing and availability.

Catalyst activity and selectivity were shown to be directly impacted by the water content in the solvent, with anhydrous operation providing the highest catalyst activity, productivity, and lifetime. Catalyst activity is sustained for ~3 h in experiments with water in the feed, with a subsequent decay in activity attributed to sorbed carbonates and CO impeding the reaction. Water content in the solvent is believed to react with captured CO_2 to form bicarbonates and carbonates (carbamate/CO_2 + H_2O → HCO_3^-/CO_3^-). These species bind strongly with the catalyst at low reaction temperatures and thus deactivate the catalyst. Oxidation of the spent catalyst at high temperature was found to help regenerate some conversion, but subsequent activity was not sustained as long as for fresh catalysts.

Ultimately, we conclude that integrated processes that capture and catalytically hydrogenate CO_2 are also chemically viable. These processes are potentially more energetically efficient and cost-effective than conventional separate capture and conversion approaches, although significant work remains to achieve commercial viability. Key process parameters will need continued efforts to achieve higher conversion rates and selectivity of desired products, in addition to establishing a catalyst water tolerance. We posit that with continued refinement, our envisioned fully closed-loop continuous IC^{3}M process can be realized. Current efforts in our laboratory are focusing on assessing optimal process conditions for the coupled processes, testing new catalyst formulations, and developing efficient methods for regenerating spent catalysts.

AUTHOR INFORMATION

Corresponding Author

David J. Heldebrant − *Pacific Northest National Laboratory, Richland, Washington 99352, United States;* orcid.org/0000-0002-5529-526X; Email: david.heldebrant@pnnl.gov

Authors

Dushyant Barpaga − *Pacific Northest National Laboratory, Richland, Washington 99352, United States;* orcid.org/0000-0003-2271-6213

Jaelynne A. King − *Pacific Northest National Laboratory, Richland, Washington 99352, United States*

Jotheeswari Kothandaraman − *Pacific Northest National Laboratory, Richland, Washington 99352, United States;* orcid.org/0000-0001-6306-9468

Johnny S. Lopez − *Pacific Northest National Laboratory, Richland, Washington 99352, United States*

Benjamin M. Moskowitz − *Pacific Northest National Laboratory, Richland, Washington 99352, United States*

Michael L. Hubbard − *Pacific Northest National Laboratory, Richland, Washington 99352, United States*

Richard F. Zheng − *Pacific Northest National Laboratory, Richland, Washington 99352, United States*

Deepika Malhotra − *Pacific Northest National Laboratory, Richland, Washington 99352, United States;* orcid.org/0000-0002-0796-6508

Phillip K. Koech − *Pacific Northest National Laboratory, Richland, Washington 99352, United States*

Andy J. Zwoster − *Pacific Northest National Laboratory, Richland, Washington 99352, United States*

Robert A. Dagle − *Pacific Northest National Laboratory, Richland, Washington 99352, United States;* orcid.org/0000-0002-8208-2163

Complete contact information is available at: https://pubs.acs.org/10.1021/acsomega.4c06919

Author Contributions

D.B. and J.A.K: data curation, formal analysis, investigation, and writing—original draft; J.K., R.F.Z., R.A.D., and D.J.H: conceptualization, funding acquisition, project administration, supervision, and writing—review and editing; J.S.L., B.M.M., M.H., D.M., P.K.K., and A.J.Z.: data curation, investigation, and methodology.

Notes

The authors declare no competing financial interest.

ACKNOWLEDGMENTS

The authors would like to acknowledge the U.S. Department of Energy (DOE) Office of Fossil Energy and Carbon

https://doi.org/10.1021/acsomega.4c06919
ACS Omega 2024, 9, 46247−46262

Management (FECM) (FWP 80562) and Southern California Gas Company for funding. The high-temperature/high-pressure solid-state NMR experiments and catalyst characterizations were performed under a user proposal at the William R. Wiley Environmental Molecular Sciences Laboratory (EMSL), which is a national scientific user facility sponsored by the DOE Office of Biological and Environmental Research and located at PNNL in Richland, Washington. The views and opinions of the authors expressed herein do not necessarily state or reflect those of the U.S. government or any agency thereof. Neither the U.S. government nor any agency thereof, nor any of their employees, makes any warranty, expressed or implied, or assumes any legal liability or responsibility for the accuracy, completeness, or usefulness of any information, apparatus, product, or process disclosed, or represents that its use would not infringe privately owned rights.

REFERENCES

(1) Al-Mamoori, A.; Krishnamurthy, A.; Rownaghi, A. A.; Rezaei, F. Carbon Capture and Utilization Update. *Energy Technol.* **2017**, *5* (6), 834−849.
(2) Bui, M.; Adjiman, C. S.; Bardow, A.; Anthony, E. J.; Boston, A.; Brown, S.; Fennell, P. S.; Fuss, S.; Galindo, A.; Hackett, L. A.; Hallett, J. P.; Herzog, H. J.; Jackson, G.; Kemper, J.; Krevor, S.; Maitland, G. C.; Matuszewski, M.; Metcalfe, I. S.; Petit, C.; Puxty, G.; Reimer, J.; Reiner, D. M.; Rubin, E. S.; Scott, S. A.; Shah, N.; Smit, B.; Trusler, J. P. M.; Webley, P.; Wilcox, J.; Mac Dowell, N. Carbon capture and storage (CCS): the way forward. *Energ Environ. Sci.* **2018**, *11* (5), 1062−1176.
(3) Gabrielli, P.; Gazzani, M.; Mazzotti, M. The Role of Carbon Capture and Utilization, Carbon Capture and Storage, and Biomass to Enable a Net-Zero-CO_2 Emissions Chemical Industry. *Ind. Eng. Chem. Res.* **2020**, *59* (15), 7033−7045.
(4) Hepburn, C.; Adlen, E.; Beddington, J.; Carter, E. A.; Fuss, S.; Mac Dowell, N.; Minx, J. C.; Smith, P.; Williams, C. K. The technological and economic prospects for CO_2 utilization and removal. *Nature.* **2019**, *575* (7781), 87−97.
(5) Leclaire, J.; Heldebrant, D. J. A call to (green) arms: a rallying cry for green chemistry and engineering for CO_2 capture, utilisation and storage. *Green Chem.* **2018**, *20* (22), 5058−5081.
(6) United Nations *For a livable climate: Net-zero commitments must be backed by credible action.* https://www.un.org/en/climatechange/net-zero-coalition#.
(7) Peplow, M. The race to upcycle CO_2 into fuels, concrete and more. *Nature.* **2022**, *603* (7903), 780−783.
(8) Ra, E. C.; Kim, K. Y.; Kim, E. H.; Lee, H.; An, K.; Lee, J. S. Recycling Carbon Dioxide through Catalytic Hydrogenation: Recent Key Developments and Perspectives. *Acs Catal.* **2020**, *10* (19), 11318−11345.
(9) Tollefson, J. Climate change is hitting the planet faster than scientists originally thought. *Nature* **2022**, DOI: . https://www.ncbi.nlm.nih.gov/pubmed/35228735
(10) National Academies of Sciences, Engineering, and Medicine; Division on Earth and Life Studies; Ocean Studies Board; Board on Chemical Sciences and Technology; Board on Earth Sciences and Resources; Board on Agriculture and Natural Resources; Board on Energy and Environmental Systems; Board on Atmospheric Sciences and Climate; Committee on Developing a Research Agenda for Carbon Dioxide Removal and Reliable Sequestration, *Negative Emissions Technologies and Reliable Sequestration: A Research Agenda*. 24. National Academies Press. 2018.
(11) IEA (2020) *CCUS in Clean Energy Transitions.* https://www.iea.org/reports/ccus-in-clean-energy-transitions.
(12) Baylin-Stern, A. B.; Berghout, N.; *Is carbon capture too expensive?* https://www.iea.org/commentaries/is-carbon-capture-too-expensive 2021.
(13) James, R.; Zoelle, A.; Keairns, D.; Turner, M.; Woods, M.; Kuehn, N. *Cost and Performance Baseline for Fossil Energy Plants Volume 1: Bituminous Coal and Natural Gas to Electricity*; 2019 NETL.
(14) Keith, D. W.; Holmes, G.; St. Angelo, D.; Heidel, K. A Process for Capturing CO_2 from the Atmosphere. *Joule* **2018**, *2* (8), 1573−1594.
(15) Aaron, D.; Tsouris, C. Separation of CO_2 from Flue Gas: A Review. *Sep. Sci. Technol.* **2005**, *40* (1−3), 321−348.
(16) Heldebrant, D. J.; Koech, P. K.; Glezakou, V. A.; Rousseau, R.; Malhotra, D.; Cantu, D. C. Water-Lean Solvents for Post-Combustion CO_2 Capture: Fundamentals, Uncertainties, Opportunities, and Outlook. *Chem. Rev.* **2017**, *117* (14), 9594−9624.
(17) Heldebrant, D. J.; Kothandaraman, J., Chapter 3 Solvent-based Absorption. In *Carbon Capture and Storage*, Bui, M.; Mac Dowell, N., Eds. Royal Society of Chemistry: 2019; pp 36−68.
(18) Luis, P. Use of monoethanolamine (MEA) for CO_2 capture in a global scenario: Consequences and alternatives. *Desalination.* **2016**, *380*, 93−99.
(19) Rochelle, G. T. Amine Scrubbing for CO_2 Capture. *Science.* **2009**, *325* (5948), 1652−1654.
(20) Samanta, A.; Zhao, A.; Shimizu, G. K. H.; Sarkar, P.; Gupta, R. Post-Combustion CO_2 Capture Using Solid Sorbents: A Review. *Ind. Eng. Chem. Res.* **2012**, *51* (4), 1438−1463.
(21) Wang, J.; Huang, L.; Yang, R.; Zhang, Z.; Wu, J.; Gao, Y.; Wang, Q.; O'Hare, D.; Zhong, Z. Recent advances in solid sorbents for CO_2 capture and new development trends. *Energ Environ. Sci.* **2014**, *7* (11), 3478−3518.
(22) Hou, R.; Fong, C.; Freeman, B. D.; Hill, M. R.; Xie, Z. Current status and advances in membrane technology for carbon capture. *Sep. Purif. Technol.* **2022**, *300*, No. 121863.
(23) Victor, N.; Nichols, C. CCUS deployment under the U.S. 45Q tax credit and adaptation by other North American Governments: MARKAL modeling results. *Computers & Industrial Engineering.* **2022**, *169*, No. 108269.
(24) Yusuf, N.; Almomani, F.; Qiblawey, H. Catalytic CO_2 conversion to C1 value-added products: Review on latest catalytic and process developments. *Fuel.* **2023**, *345*, No. 128178.
(25) Peter, S. C. Reduction of CO_2 to Chemicals and Fuels: A Solution to Global Warming and Energy Crisis. *ACS Energy Lett.* **2018**, *3* (7), 1557−1561.
(26) Saravanan, A.; Senthil kumar, P.; Vo, D.-V. N.; Jeevanantham, S.; Bhuvaneswari, V.; Anantha Narayanan, V.; Yaashikaa, P. R.; Swetha, S.; Reshma, B. A comprehensive review on different approaches for CO_2 utilization and conversion pathways. *Chem. Eng. Sci.* **2021**, *236*, No. 116515.
(27) Kothandaraman, J.; Heldebrant, D. J. Catalytic Co-production of Methanol and Glycol in One Pot from Epoxide. *RSC Adv.* **2020**, *10*, 42557−42563.
(28) Klankermayer, J.; Leitner, W. Love at second sight for CO_2 and H_2 in organic synthesis. *Science.* **2015**, *350* (6261), 629−30.
(29) Klankermayer, J.; Wesselbaum, S.; Beydoun, K.; Leitner, W. Selective Catalytic Synthesis Using the Combination of Carbon Dioxide and Hydrogen: Catalytic Chess at the Interface of Energy and Chemistry. *Angew. Chem., Int. Ed.* **2016**, *55* (26), 7296−343.
(30) Liu, Q.; Wu, L.; Jackstell, R.; Beller, M. Using carbon dioxide as a building block in organic synthesis. *Nat. Commun.* **2015**, *6*, 5933.
(31) Olah, G. A.; Goeppert, A.; Prakash, G. K. Chemical recycling of carbon dioxide to methanol and dimethyl ether: from greenhouse gas to renewable, environmentally carbon neutral fuels and synthetic hydrocarbons. *J. Org. Chem.* **2009**, *74* (2), 487−98.
(32) Olah, G. A.; Prakash, G. K.; Goeppert, A. Anthropogenic chemical carbon cycle for a sustainable future. *J. Am. Chem. Soc.* **2011**, *133* (33), 12881−98.
(33) Sakakura, T.; Choi, J. C.; Yasuda, H. Transformation of carbon dioxide. *Chem. Rev.* **2007**, *107* (6), 2365−87.
(34) Scott, M.; Westhues, C. G.; Kaiser, T.; Baums, J. C.; Jupke, A.; Francio, G.; Leitner, W. Methylformate from CO_2: an integrated process combining catalytic hydrogenation and reactive distillation. *Green Chem.* **2019**, *21* (23), 6307−6317.

https://doi.org/10.1021/acsomega.4c06919
ACS Omega 2024, 9, 46247−46262

(35) Song, C. Global challenges and strategies for control, conversion and utilization of CO_2 for sustainable development involving energy, catalysis, adsorption and chemical processing. *Catal. Today.* **2006**, *115*, 2−32.
(36) Sternberg, A.; Jens, C. M.; Bardow, A. Life cycle assessment of CO_2-based C1-chemicals. *Green Chem.* **2017**, *19* (9), 2244−2259.
(37) van Bavel, S.; Verma, S.; Negro, E.; Bracht, M. Integrating CO_2 Electrolysis into the Gas-to-Liquids−Power-to-Liquids Process. *ACS Energy Lett.* **2020**, *5* (8), 2597−2601.
(38) Zhang, Z.; Wang, T.; Blunt, M. J.; Anthony, E. J.; Park, A.-H. A.; Hughes, R. W.; Webley, P. A.; Yan, J. Advances in carbon capture, utilization and storage. *Appl. Energy.* **2020**, *278*, No. 115627.
(39) Heldebrant, D. J.; Kothandaraman, J.; Dowell, N. M.; Brickett, L. Next steps for solvent-based CO_2 capture; integration of capture, conversion, and mineralisation. *Chem. Sci.* **2022**, *13* (22), 6445−6456.
(40) Lao, D. B.; Galan, B. R.; Linehan, J. C.; Heldebrant, D. J. The steps of activating a prospective CO_2 hydrogenation catalyst with combined CO_2 capture and reduction. *Green Chem.* **2016**, *18* (18), 4871−4874.
(41) Kothandaraman, J.; Dagle, R. A.; Dagle, V. L.; Davidson, S. D.; Walter, E. D.; Burton, S. D.; Hoyt, D. W.; Heldebrant, D. J. Condensed-phase low temperature heterogeneous hydrogenation of CO_2 to methanol. *Catal. Sci. Technol.* **2018**, *8*, 5098−5103.
(42) Xie, S.; Zhang, W.; Lan, X.; Lin, H. CO_2 Reduction to Methanol in the Liquid Phase: A Review. *Chemsuschem.* **2020**, *13* (23), 6141−6159.
(43) Kar, S.; Goeppert, A.; Prakash, G. K. S. Integrated CO_2 Capture and Conversion to Formate and Methanol: Connecting Two Threads. *Acc. Chem. Res.* **2019**, *52* (10), 2892−2903.
(44) Rezayee, N. M.; Huff, C. A.; Sanford, M. S. Tandem amine and ruthenium-catalyzed hydrogenation of CO_2 to methanol. *J. Am. Chem. Soc.* **2015**, *137* (3), 1028−31.
(45) Kothandaraman, J.; Heldebrant, D. J. Towards environmentally benign capture and conversion: heterogeneous metal catalyzed CO_2 hydrogenation in CO_2 capture solvents. *Green Chem.* **2020**, *22* (3), 828−834.
(46) Scott, M.; Blas Molinos, B.; Westhues, C.; Francio, G.; Leitner, W. Aqueous Biphasic Systems for the Synthesis of Formates by Catalytic CO_2 Hydrogenation: Integrated Reaction and Catalyst Separation for CO_2 -Scrubbing Solutions. *Chemsuschem.* **2017**, *10* (6), 1085−1093.
(47) Kothandaraman, J.; Zhang, J.; Glezakou, V.-A.; Mock, M. T.; Heldebrant, D. J. Chemical transformations of captured CO_2 into cyclic and polymeric carbonates. *J. CO2 Utili.* **2019**, *32*, 196−201.
(48) Maina, J. W.; Pringle, J. M.; Razal, J. M.; Nunes, S.; Vega, L.; Gallucci, F.; Dumee, L. F. Strategies for Integrated Capture and Conversion of CO_2 from Dilute Flue Gases and the Atmosphere. *Chemsuschem.* **2021**, *14* (8), 1805−1820.
(49) Jakobsen, J. B.; Ronne, M. H.; Daasbjerg, K.; Skrydstrup, T. Are Amines the Holy Grail for Facilitating CO_2 Reduction? *Angew. Chem., Int. Ed.* **2021**, *60* (17), 9174−9179.
(50) Bi, J.; Hou, P.; Liu, F. W.; Kang, P. Electrocatalytic Reduction of CO_2 to Methanol by Iron Tetradentate Phosphine Complex Through Amidation Strategy. *Chemsuschem.* **2019**, *12* (10), 2195−2201.
(51) Yadav, M.; Linehan, J. C.; Karkamkar, A. J.; van der Eide, E.; Heldebrant, D. J. Homogeneous hydrogenation of CO_2 to methyl formate utilizing switchable ionic liquids. *Inorg. Chem.* **2014**, *53* (18), 9849−54.
(52) Wilson, E. A. K.; Eady, S. C.; Silbaugh, T.; Thompson, L. T.; Barteau, M. A. Both sites must turn over in tandem catalysis: Lessons from one-pot CO_2 capture and hydrogenation. *J. Catal.* **2021**, *404*, 977−984.
(53) Ni, S.; Zhu, J.; Roy, R.; Li, C.-J.; Lennox, R. B. Catalytic hydrogenation of CO_2 from air via porous silica-supported Au nanoparticles in aqueous solution. *Green Chem.* **2021**, *23*, 3740−3749.
(54) Lu, M.; Zhang, J.; Yao, Y.; Sun, J.; Wang, Y.; Lin, H. Renewable energy storage via efficient reversible hydrogenation of piperidine captured CO_2. *Green Chem.* **2018**, *20* (18), 4292−4298.
(55) Khusnutdinova, J. R.; Garg, J. A.; Milstein, D. Combining Low-Pressure CO_2 Capture and Hydrogenation To Form Methanol. *Acs Catal.* **2015**, *5* (4), 2416−2422.
(56) McNamara, N. D.; Hicks, J. C. CO_2 capture and conversion with a multifunctional polyethyleneimine-tethered iminophosphine iridium catalyst/adsorbent. *Chemsuschem.* **2014**, *7* (4), 1114−24.
(57) Reller, C.; Poge, M.; Lissner, A.; Mertens, F. O. Methanol from CO_2 by organo-cocatalysis: CO_2 capture and hydrogenation in one process step. *Environ. Sci. Technol.* **2014**, *48* (24), 14799−804.
(58) Overa, S.; Feric, T. G.; Park, A.-H. A.; Jiao, F. Tandem and Hybrid Processes for Carbon Dioxide Utilization. *Joule.* **2021**, *5* (1), 8−13.
(59) Wei, D.; Junge, H.; Beller, M. An amino acid based system for CO_2 capture and catalytic utilization to produce formates. *Chem. Sci.* **2021**, *12* (17), 6020−6024.
(60) Wei, D.; Sang, R.; Moazezbarabadi, A.; Junge, H.; Beller, M. Homogeneous Carbon Capture and Catalytic Hydrogenation: Toward a Chemical Hydrogen Battery System. *JACS Au.* **2022**, *2* (5), 1020−1031.
(61) Kar, S.; Goeppert, A.; Kothandaraman, J.; Prakash, G. K. S. Manganese-Catalyzed Sequential Hydrogenation of CO_2 to Methanol via Formamide. *Acs Catal.* **2017**, *7* (9), 6347−6351.
(62) Kothandaraman, J.; Lopez, J. S.; Jiang, Y.; Walter, E. D.; Burton, S. D.; Dagle, R. A.; Heldebrant, D. J. Integrated Capture and Conversion of CO_2 to Methane Using a Water-lean, Post-Combustion CO_2 Capture Solvent. *Chemsuschem* **2021**, *14* (21), 4812−4819.
(63) Kothandaraman, J.; Goeppert, A.; Czaun, M.; Olah, G. A.; Surya Prakash, G. K. CO_2 capture by amines in aqueous media and its subsequent conversion to formate with reusable ruthenium and iron catalysts. *Green Chemistry.* **2016**, *18* (21), 5831−5838.
(64) Kothandaraman, J.; Goeppert, A.; Czaun, M.; Olah, G. A.; Prakash, G. K. S. Conversion of CO_2 from Air into Methanol Using a Polyamine and a Homogeneous Ruthenium Catalyst. *J. Am. Chem. Soc.* **2016**, *138* (3), 778−781.
(65) Freyman, M. C.; Huang, Z.; Ravikumar, D.; Duoss, E. B.; Li, Y.; Baker, S. E.; Pang, S. H.; Schaidle, J. A. Reactive CO_2 capture: A path forward for process integration in carbon management. *Joule.* **2023**, *7* (4), 631−651.
(66) Kothandaraman, J.; Lopez, J. S.; Jiang, Y.; Walter, E. D.; Burton, S. D.; Dagle, R. A.; Heldebrant, D. J. Integrated Capture and Conversion of CO_2 to Methanol in a Post-Combustion Capture Solvent: Heterogeneous Catalysts for Selective C-N Bond Cleavage. *Adv. Energy Mater.* **2022**, *12* (46), No. 2202369.
(67) Cantu, D. C.; Malhotra, D.; Nguyen, M.-T.; Koech, P. K.; Zhang, D.; Glezakou, V.-A.; Rousseau, R.; Page, J.; Zheng, R.; Perry, R. J.; Heldebrant, D. J. Molecular-Level Overhaul of γ-Aminopropyl Aminosilicone/Triethylene Glycol Post-Combustion CO_2-Capture Solvents. *Chemsuschem.* **2020**, *13* (13), 3429−3438.
(68) Barpaga, D.; Jiang, Y.; Zheng, R. F.; Malhotra, D.; Koech, P. K.; Zwoster, A.; Mathias, P. M.; Heldebrant, D. J. Evaluation of a Third Generation Single-Component Water-Lean Diamine Solvent for Post-Combustion CO_2 Capture. *Acs Sustain Chem. Eng.* **2022**, *10* (14), 4522−4528.
(69) Zheng, R. F.; Barpaga, D.; Mathias, P. M.; Malhotra, D.; Koech, P. K.; Jiang, Y.; Bhakta, M.; Lail, M.; Rayer, A. V.; Whyatt, G. A.; Freeman, C. J.; Zwoster, A. J.; Weitz, K. K.; Heldebrant, D. J. A single-component water-lean post-combustion CO_2 capture solvent with exceptionally low operational heat and total costs of capture - comprehensive experimental and theoretical evaluation. *Energy Environ. Sci.* **2020**, *13* (11), 4106−4113.
(70) Lines, A. M.; Barpaga, D.; Zheng, R. F.; Collett, J. R.; Heldebrant, D. J.; Bryan, S. A. In Situ Raman Methodology for Online Analysis of CO_2 and H_2O Loadings in a Water-Lean Solvent for CO_2 Capture. *Anal. Chem.* **2023**, *95* (42), 15566−15576.
(71) Grabow, L. C.; Gokhale, A. A.; Evans, S. T.; Dumesic, J. A.; Mavrikakis, M. Mechanism of the water gas shift reaction on Pt: First principles, experiments, and microkinetic modeling. *J. Phys. Chem. C* **2008**, *112* (12), 4608−4617.

https://doi.org/10.1021/acsomega.4c06919
ACS Omega 2024, 9, 46247−46262

(72) Grenoble, D. C.; Estadt, M. M.; Ollis, D. F. The Chemistry and Catalysis of the Water Gas Shift Reaction 0.1. The Kinetics over Supported Metal-Catalysts. *J. Catal.* **1981**, *67* (1), 90−102.
(73) Mino, L.; Spoto, G.; Ferrari, A. M. CO_2 Capture by TiO_2 Anatase Surfaces: A Combined DFT and FTIR Study. *J. Phys. Chem. C* **2014**, *118* (43), 25016−25026.

https://doi.org/10.1021/acsomega.4c06919
ACS Omega 2024, 9, 46247−46262